Available online at www.sciencedirect.com
ScienceDirect
Magnetic Resonance Imaging xx (2009) xxx–xxx
MAGNETIC RESONANCE IMAGING

Quantitative intact specimen magnetic resonance microscopy at 3.0 T☆

Kevin G. Bath[a,*], Henning U. Voss[b], Deqiang Jing[a], Stewart Anderson[a], Barbara Hempstead[d], Francis S. Lee[a], Jonathan P. Dyke[b], Douglas J. Ballon[b,c,*]

[a]Department of Psychiatry, Weill Cornell Medical College of Cornell University, 1300 York Avenue, New York, NY 10065, USA
[b]Department of Radiology, Weill Cornell Medical College of Cornell University, 1300 York Avenue, New York, NY 10065, USA
[c]Department of Physiology, Biophysics, and Systems Biology, Weill Graduate School of Medical Sciences, Cornell University, 1300 York Avenue, New York, NY 10065, USA
[d]Division of Hematology and Medical Oncology, Department of Medicine, Weill Cornell Medical College of Cornell University, 1300 York Avenue, New York, NY 10065, USA

Received 18 June 2008; revised 4 November 2008; accepted 10 November 2008

Abstract

In this report, we discuss the application of a methodology for high-contrast, high-resolution magnetic resonance microscopy (MRM) of murine tissue using a 3.0-T imaging system. We employed a threefold strategy that included customized specimen preparation to maximize image contrast, three-dimensional data acquisition to minimize scan time and custom radiofrequency resonator design to maximize signal sensitivity. Images had a resolution of 100×78×78 μm^3 with a signal-to-noise ratio per voxel greater than 25:1 and excellent contrast-to-noise ratios over a 30-min acquisition. We quantitatively validated the methods through comparisons of neuroanatomy across two lines of genetically engineered mice. Specifically, we were able to detect volumetric differences of as little as 9% between genetically engineered mouse strains in multiple brain regions that were predictive of underlying impairments in brain development. The overall methodology was straightforward to implement and provides ready access to basic MRM at field strengths that are widely available in both the laboratory and the clinic.

Keywords: Magnetic resonance microscopy (MRM); Mouse; Neuroanatomy; TrkB; FoxG1

1. Introduction

The ongoing development of genetically engineered mice as models for human pathology and a means to understand gene function has generated a growing need for a rapid and accurate means of anatomical phenotyping. Magnetic resonance microscopy (MRM) has been used to assess intact murine anatomy while avoiding many of the problems associated with standard histological procedures, such as uneven sections, realignment during volume reconstruction and tissue shrinkage during processing [1,2]. The initial development of MRM as well as early applications was conducted with magnetic field strengths as low as 1.5 to 3.0 T, but more recently field strengths greater than 10 T have yielded greatly enhanced intrinsic signal sensitivity [3–6].

Given these results, it is important to note that the criteria governing the success of an MRM study may not depend critically upon the magnetic field strength in all cases. First and foremost, the methods must provide adequate sensitivity over the data acquisition period for resolution of structures of interest. This criterion implies that higher fields are preferable, but it is also clear that resolution should be selected based primarily upon the spatial frequencies of the structure under study. It is also true that adequate image contrast must be achieved such that boundaries between tissues or regions of interest within tissue can be accurately delineated. Since in many cases nuclear relaxation times are better differentiated at lower field strengths [7], this criterion

☆ This work was supported by the Sackler Institute (KGB, FSL), DeWitt-Wallace Fund of the New York Community Trust (FSL), NARSAD (FSL) and NIH (MH060478-KGB, NS052819-FSL, MH068850-FSL, NS30687-BLH), National Institute of Biomedical Imaging and Bioengineering (EB002070-DJB).

* Corresponding authors.
E-mail addresses: kgb2001@med.cornell.edu (K.G. Bath), djb2001@med.cornell.edu (D.J. Ballon).

0730-725X/$ – see front matter © 2009 Elsevier Inc. All rights reserved.
doi:10.1016/j.mri.2008.11.008

actually suggests that *lower* field systems may be advantageous under certain conditions [8]. Third, rapid acquisition of images is highly advantageous in order for high throughput studies to be both economically and practically feasible. In this case, strong magnetic field gradients can be critical for overcoming magnetic susceptibility-related image distortion and signal loss, but since the magnetic susceptibility effects are proportional to field strength, the necessary gradient strength also scales linearly with the field. In addition, the wide magnet bores of lower field systems are amenable to parallel imaging of multiple animals. Finally, at higher field strengths the specific absorption rate of introduced electromagnetic energy increases, placing limits upon radiofrequency pulse power and repetition times.

In this report, we detail a technique for the acquisition of high spatial resolution images using a 3.0-T imaging system in only 30 min, with both signal-to-noise and contrast-to-noise ratios (SNR and CNR, respectively) typically greater than 25:1 for defined regions of interest [9]. Specifically, using the methods described here it was possible to identify differences in substructural volumes in the murine brain as small as 10%. We quantitatively validated the methodology through a comparison of hippocampal volume measurements obtained via MRM vs. standard histological procedures. In addition, we segmented multiple brain regions and compared regional volumes between genetically engineered mouse models of compromised neurogenesis. The techniques described here can be easily and quickly adapted to nearly any MR clinical imaging platform.

2. Materials and methods

2.1. Animals

For initial validation of the techniques, wild-type C57BL/6 mice were used (n=14). For comparison of genetically engineered lines of mice, FoxG1 heterozygous "knock-in" mouse lines were used in which C57BL/6 mice had the intronless FoxG1 coding region replaced with tetracycline transactivator (tTA) (FoxG1/tTA) ($FoxG1^{+/+}$, n=4, mean weight=15.2 g; $FoxG1^{+/-}$, n= 4, mean weight=12.3 g) [10]. As a more demanding test of the methodology, TrkB heterozygous null lines of mice were maintained on a C57BL/6 background ($TrkB^{+/+}$, n=4, mean weight=30.8 g; $TrkB^{+/-}$, n=4, mean weight=37.5 g) [11]. FoxG1 mice were between 5 and 6 weeks of age and all other mice were 8- to 10-week-old adult animals.

2.2. Sample preparation

Mice were first deeply anesthetized with pentobarbital. The thoracic cavity was then opened exposing the heart, and animals were intracardially perfused with a solution of 0.9% saline, 0.1% sodium nitrite and 5% gadolinium-DTPA (Magnevist, Berlex Laboratories, Wayne, NJ, USA) followed by a solution of 4% paraformaldehyde and 5% Magnevist in phosphate buffered saline (PBS). The final concentration of gadolinium-DTPA in perfusion solutions was 46.91 mg/ml. Perfusates were administered at a rate of 5 ml/min using a silastic pump. Subsequently, the brain was resected and either postfixed in a 4% paraformaldehyde and 5% Magnevist solution or stored in a 0.1-M PBS solution containing 5% Magnevist for 3–7 days prior to imaging.

2.3. Radiofrequency resonators

A Hoult-Deslauriers modular radiofrequency resonator design was used consisting of five inductively coupled, 11-mm-diameter resonant loops arranged in a cylindrical geometry of length 20 mm with an inductively coupled drive loop placed at one end (Fig. 1A, B) [12]. We used 62-pF porcelain chip capacitors (American Technical Ceramics) on each of the loops with the exception of the center loop, on which a 30-pF fixed capacitor was placed in parallel with a 5- to 40-pF variable mini-trimmer capacitor (Johanson 9341-9SL) that afforded a tuning range for the entire structure of approximately 10 MHz without significant perturbations in the radiofrequency excitation (B_1) field as determined via image uniformity in a plane containing the axis of cylindrical symmetry. Adhesive-backed copper tape cut into 3-mm-wide strips was used as the conductor for each loop. The inductive drive loop had an 82-pF fixed capacitor in series to avoid a DC short of the circuit, and the loop and capacitor were both connected to a low-noise 50-Ω coaxial cable (Belden 9223). The structure belongs to a class of resonators that is well understood both theoretically and experimentally [12,13]. The lowest eigenmode was tuned to the nuclear magnetic resonance frequency for protons at 3.0 T (127.73 MHz), matched to a 50-Ω impedance with each specimen in place and produced a magnetic field profile well suited for imaging (Fig. 1C). A primary advantage of this design is that the resonators could be easily built and implemented to provide high sensitivity with no additional changes to the existing hardware or software of the scanner, with the exception of the image reconstruction scale factor and a radiofrequency power attenuator at the input to the main amplifier. This class of ladder networks can be understood using a highly compact formalism through consideration of a recursion relation for Kirchhoff's voltage equations on element n:

$$(\omega L - 1/\omega C)I_n + \kappa\omega L(I_{n+1} + I_{n-1}) = 0, \quad (1)$$

where L is the inductance on each loop element due to the copper conductors, and C is the capacitance on each loop element, I_n is the current amplitude for the nth element, κ is the coefficient of mutual inductance between nearest neighbor elements, and $\omega=2\pi\nu$ is the angular frequency of current oscillations.

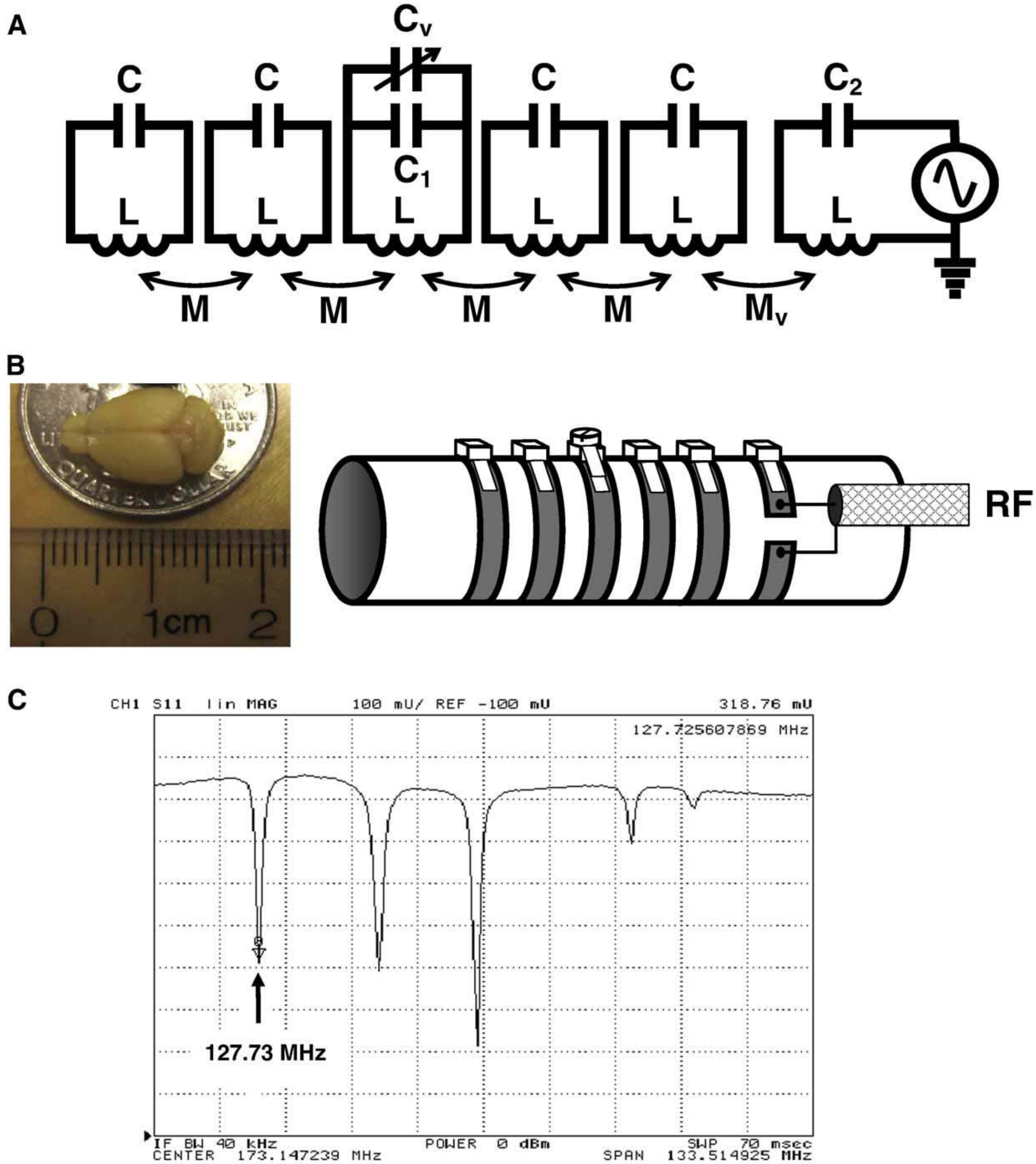

Fig. 1. The inductively coupled solenoidal radiofrequency resonator design. (A) Circuit diagram of the resonator showing the five individual resonant loops coupled via mutual inductance and driven with an inductively coupled drive loop. Capacitor values were as follows: C=62 pF, C_1=30 pF, C_2=30 pF and C_v=5–40 pF. Adjustment of the distance between the drive loop and the resonator facilitated matching of the resonator with the 50-Ω transmission line leading to the RF transmitter and receiver (not shown). (B) A fixed specimen of the murine brain and sketch of the resonator showing the positions of the capacitors, drive loop and transmission line. (C) The resonant mode spectrum of the five-element resonator. The five discrete modes predicted from the dispersion relation are visible, but only the lowest in frequency produces a field profile with all elements oscillating in phase and therefore most suitable for imaging.

Eq. (1) completely defines the eigenvalue problem for the resonator assuming no radiative or resistive losses and simple boundary conditions of the form $I_0=I_N=0$. Trial solutions of the form $I_n=A\sin(n\pi\Gamma/(N+1))$, where A is a global current amplitude on the resonator determined by the magnitude of the driving voltage, and Γ is an integer representing the resonant mode number, then lead immediately to a dispersion relation given by:

$$\omega^2=(LC)^{-1}(1+2\kappa\cos(\pi\Gamma/(N+1)))^{-1}. \quad (2)$$

The lowest of five predicted resonant modes produces the most homogeneous radiofrequency excitation field (B_1 field). All modes were observed experimentally and the lowest was used for all imaging studies. Since the B_1 field is only a weakly varying function of small perturbations of the capacitance on each element, the resonator was tuned to the operating frequency using the mini-trimmer capacitor on the center loop. Impedance matching to the 50-Ω transmission line was easily accomplished by adjustment of the distance between the drive loop and the resonator. A mounting platform was designed such that the specimens were positioned at the magnet isocenter during imaging.

2.4. Imaging

All image data were acquired on a 3.0-T magnetic resonance imaging system (GE Medical Systems, Milwaukee, WI, USA) equipped with 50 mT/m gradients operating at 150 mT/m per millisecond. The system was equipped with software version E2.0-M4-0502.b. The three-dimensional magnetization-prepared rapid gradient echo (MP-RAGE) [14] pulse sequence had the following parameters for whole brain coverage: pulse repetition time=20.3 ms, inversion time=725.0 ms, echo time=9.6 ms, field-of-view=1×2 cm, slice thickness=100 μm, matrix size=128×256×60-76, flip angle=60° and number of averages=4. The above parameters yielded a spatial resolution of 100×78×78 μm. In addition, it was possible to view all images at half the SNR in approximately 8 min using a single acquisition. This feature allowed fast prototyping of the resonators and sample preparation methods, but also yielded useful gross anatomical features.

2.5. Image post-processing and volumetrics

Image files were stored in DICOM (Digital Imaging and Communications in Medicine, Rosslyn, VA, USA) format on an off-line server. The DICOM datasets were analyzed using Osirix software (The Osirix Foundation, Geneva, Switzerland) with the observer blind to the genotype of the specimens. Anatomical boundaries for all brain structures were checked in reference to a mouse brain atlas [15]. As an example, for the hippocampus, the external capsule, alveus of hippocampus and white matter were used as boundary landmarks. Two- and three-dimensional renderings and animations of the MP-RAGE datasets were generated using MRIcro (Chris Rorden), Irfanview (Irfan Skiljan) and GIFAnimator (Microsoft, Inc.) freeware.

2.6. Volume estimation of the hippocampus via histology

Following imaging, brains were infused with 30% sucrose and then cut at 40 μm on a freezing microtome. Every third section was mounted, stained with cresyl violet and then dehydrated for use in stereological estimation of volume. With the Steroinvestigator software (Microbrightfield, USA), the entire volume of the hippocampus was measured at 4× objective magnification. The external capsule, alveus of the hippocampus and white matter were used as boundary landmarks. All sections throughout each hippocampus were traced and reconstructed, and the Cavalieri estimator function was used to calculate the volume [16].

2.7. BrdU labeling and detection

To quantify adult neurogenesis, 5-bromo-2′-deoxyuridine (BrdU, 10 mg/ml; Sigma), a marker taken up during DNA synthesis, was administered through intraperitoneal injection in mice [$TrkB^{+/+}$ (n=4) and $TrkB^{+/-}$ (n=4), as described above] between the ages of postnatal day 60 and 90 (150 mg/kg of body weight in 0.9% NaCl). Animals were perfused 28 days following BrdU injection to track the survival of newly born cells. Following imaging, brains were infused with a 30% sucrose solution and then sectioned on a freezing microtome and then processed for immunohistochemistry. To denature DNA, sections were treated for 20 min at room temperature followed by 20 min at 37°C with 2 M HCl in PBS. Tissue was then washed in sodium borate buffer for 10 min (0.1 M, pH 8.5) and then rinsed with 0.1 M PBS before blocking and subsequent incubation with anti-BrdU antibody (for single labeling: mouse anti-BrdU 1:100; Becton Dickinson, for double labeling: mouse anti-NeuN 1:1000; Chemicon, rat anti-BrdU 1:100; Dako). The anti-BrdU antibody was then revealed either with a biotinylated secondary (goat anti-mouse 1:200; Vector Labs), ABC (Vector Labs, ABC Elite kit) and DAB peroxidase method (DAB tablet set, Sigma), or a corresponding fluorescent-labeled secondary antibody (alexa conjugated goat anti-rat 488; Molecular Probes, or alexa conjugated goat anti-mouse 594; Molecular Probes), and only immunopositive nuclei were counted.

2.8. BrdU quantitative analyses

To quantify the density of BrdU-positive cells in the granule cell layer of the olfactory bulb (OB), an optical fractionator method was used. Every third serially obtained section (80 μm interval) was mounted and processed immunohistochemically to detect BrdU. Sections were counterstained with Nissl and a reference volume of the granule cell layer was traced using a stereology system (Stereoinvestigator, Microbrightfield). BrdU-positive nuclei were counted within a 20×20×30-μm counting frame, which was randomly sampled within a 122.8×68.9-μm counting grid using a meander scanning technique. BrdU-positive cells throughout the z-plane were counted and those that contacted the lateral or upper exclusion plane remained uncounted. The total number of cells counted was divided by the number of counting frames sampled multiplied by the size of the counting frame in order to obtain an estimate of the density of BrdU-positive cells within this structure.

2.9. Animal welfare statement

The animal protocol for studies of mice was reviewed and approved by the Institutional Animal Care and Use Committee at Weill Cornell Medical College.

2.10. Statistical analyses

Means and standard errors were calculated for hippocampal volumes obtained via both MRM and histology. For comparisons of measurements obtained within the same brain, paired sample *t* tests were utilized assuming equal variance. For group comparisons between volumes obtained from genetically engineered mouse lines, means were compared using Student's *t* test for small samples assuming equal variance. Data were analyzed using SPSS software (SPSS Inc., Chicago, IL, USA) with a significance level of α=0.05.

3. Results and discussion

3.1. Assessment of image quality

From first principles, it is possible to estimate the relative quality of the images acquired in this study. We use as a benchmark images acquired at 9.4 T at a spatial resolution of 40×40×40 μm in 2 h with an SNR of 25:1 per voxel [17]. From our dataset, assuming that the pulse sequence acquisition parameters and nuclear relaxation times are the same at both field strengths, and that the signal sensitivity varies roughly linearly with field strength, we would then expect an SNR of approximately 20:1. The CNR will then be less than or equal to 20:1 based upon the specific anatomical regions of interest. The SNR estimate is close to the observed values in this study. For example, as shown in Figs. 2B and 3A, the SNR in the hippocampus is approximately 25:1, and the CNR is nearly equal to the SNR for the CA1/CA3 cell layer, since it presents a very low signal relative to adjacent hippocampal parenchyma. The remaining question is whether the acquired image resolution at 3.0 T is sufficient to both visualize and quantify structures of interest. This will be demonstrated below for several structures within the murine brain.

The superparamagnetic contrast agent gadopentetate dimeglumine (Gd-DTPA), which is routinely used in clinical magnetic resonance imaging, has also been adapted for MRM [17]. In the present study, both the SNR and the CNR in tissue were enhanced via a 96-h marination of each specimen in a 5% solution of Gd-DTPA in PBS. A high

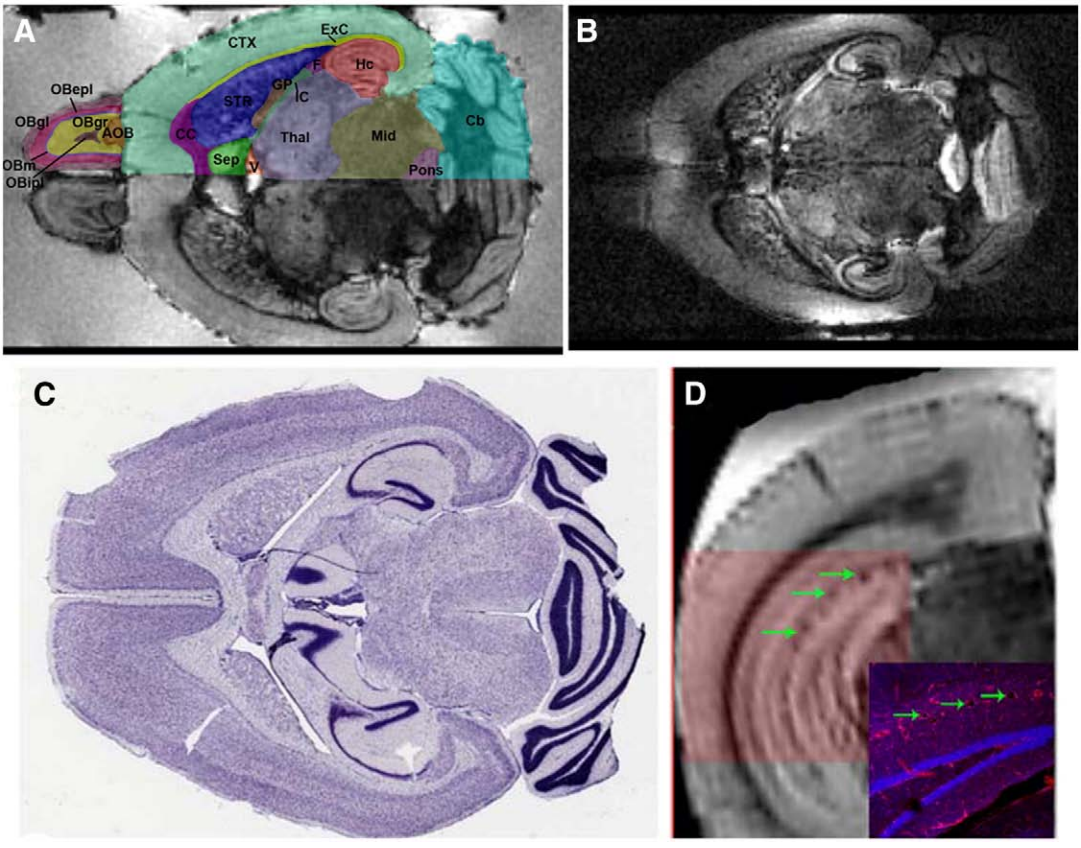

Fig. 2. Murine neuroanatomy obtained via MRM at 3.0 T. (A,B) Datasets obtained in 30 min using (A) Gd-DTPA-infused saline or (B) Gd-DTPA-infused saline followed by substitution with deuterated water. (C) Comparison with a Nissl-stained histological section. (D) Coronal brain image showing blood vessels in the hippocampus (green arrows) and (inset) a comparable histologically prepared section labeled with isolectin B-4 (red — a marker for vasculature) and counterstained with TO-PRO3 (blue).

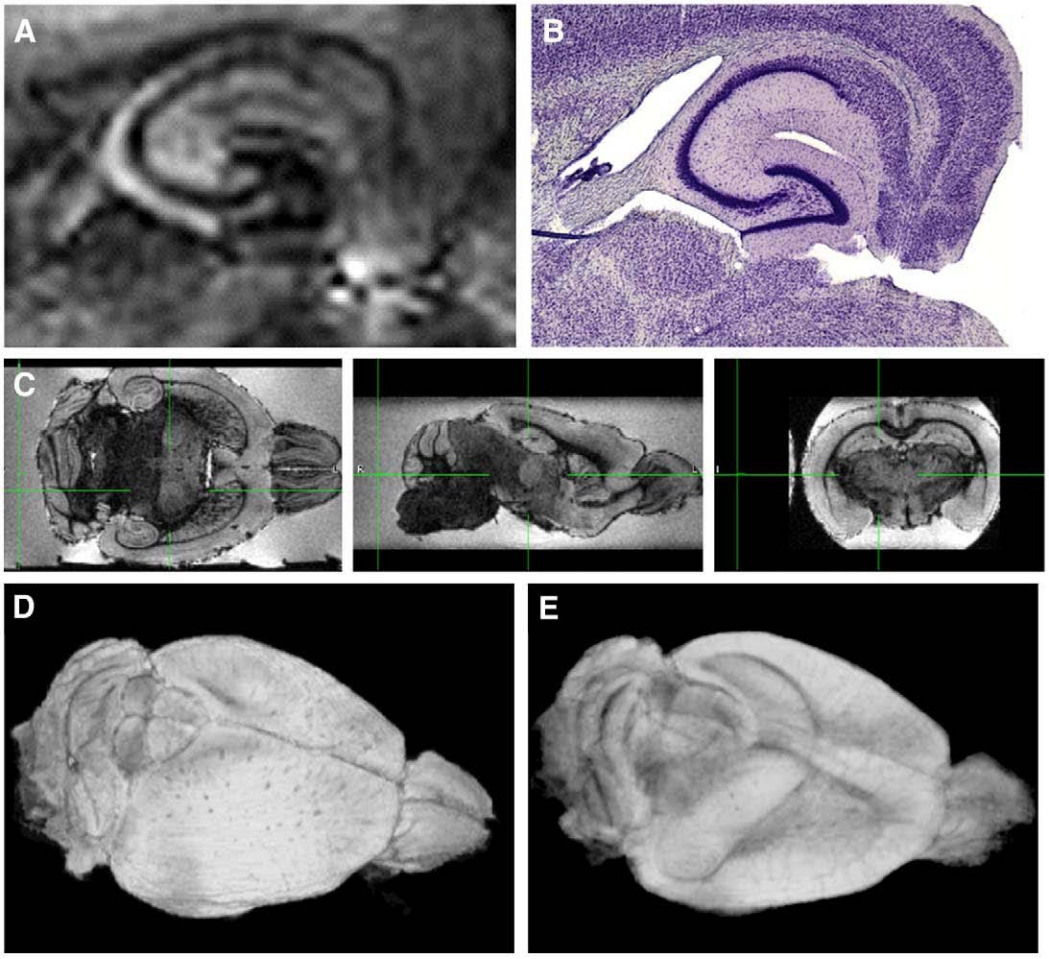

Fig. 3. MRM of hippocampal anatomy. (A) Image of murine hippocampus clearly showing the cell layers CA1, CA3 and the dentate gyrus (DG) of the hippocampus. The image was interpolated to a 1024×1024 matrix before cropping. (B) Corresponding histological section. (C) 3.0-T, 30-min MRM of the mouse brain in three planes from the MP-RAGE dataset. (D) Surface and (E) partially transparent mean intensity plot of regions probed for volumetric analysis, including the OB, cerebral cortex, cerebellum and hippocampus. Close inspection of both images reveals significant neurovascular architecture.

CNR was critical for clear delineation of boundaries within samples and for comparison of differences between regions of interest across samples. It was also observed that the CNR was a sensitive function of the marination process and could for example be altered by substitution of water (H_2O) with deuterated water (D_2O). This is demonstrated through the comparison of a brain imaged in gadolinium-infused saline (Fig. 2A) or substitution of the carrier media with 95% D_2O (Fig. 2B), which resulted in a markedly different outcome while using the same tissue preparation procedures, imaging sequence and acquisition parameters. Images were compared to histologically prepared tissue sections and demonstrated a high degree of anatomical fidelity (Fig. 2C). MRM images could be segmented into numerous easily identifiable structures (Fig. 2A). Furthermore, by combining sodium nitrite in the perfusates at the time of sacrifice, blood vessels were kept patent, which allowed for imaging of vasculature within tissues of interest (Figs. 2D and 3D, E), thus demonstrating the potential utility of this methodology for angiography.

3.2. Validation for use in morphological phenotyping

A primary goal of this work was to determine the utility of this methodology as a means to rapidly and accurately quantify morphological features of specific tissues. In studies of the excised mouse brain, images obtained using the above procedures allowed for the accurate identification of substructural detail in the hippocampus (Fig. 3A and B). The acquisition of nearly isotropic datasets allowed reformatting of images in any plane while retaining the integrity of the display (Fig. 3C) and also facilitated three-dimensional reconstruction of tissues of interest (Fig. 3D and E).

Hippocampal volume measurements using MRM were significantly correlated with those obtained from histological preparations (R^2=0.286, P<.05). The methodologies were found to differ by an average of less than 6% (±2 S.E.M.; Fig. 4A). To then determine the reliability of measurements obtained via MRM, we assessed both measure–remeasure reliability (within-rater) and inter-rater reliability (indepen-

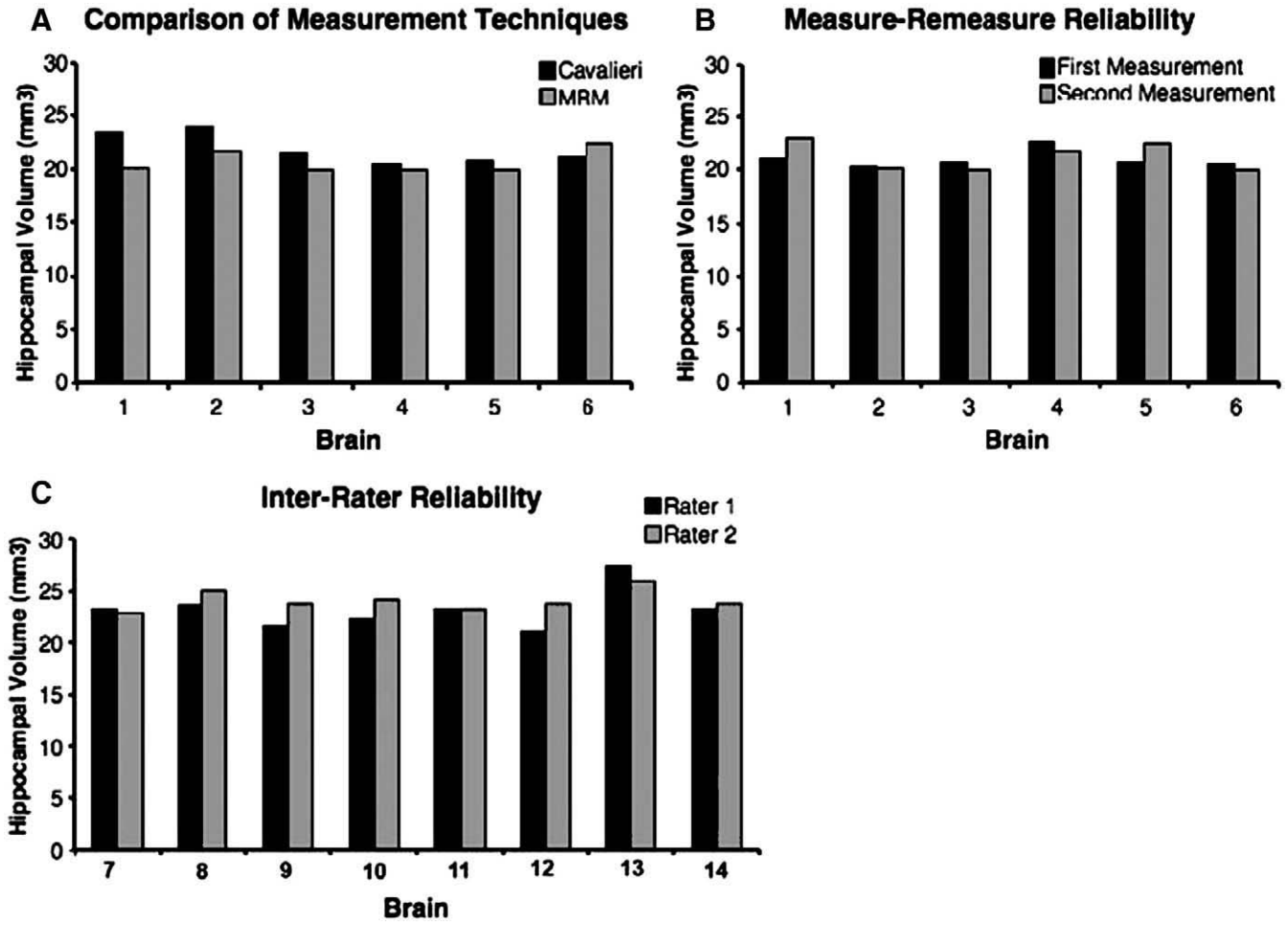

Fig. 4. Comparison of 3.0-T MRM to standard histological techniques. Bar graphs depicting hippocampal volume measurements obtained from individual brains of wild-type C57BL/6 mice for (A) comparison between MRM and histology (n=6), (B) measure–remeasure reliability [n=6, same cohort as in (A)] and (C) inter-rater reliability for volume measurements from a second set of brains (n=8).

dent raters) for hippocampal volume measurements. We found both within-rater and between-rater measurements to be highly reliable (Fig. 4B and C), with the within-rater measurements being significantly correlated (R^2=0.402, P<05) differing on average from the first to second measurement by 1% (±2.4 S.E.M.; Fig. 4B). For between-rater measurements, we also found a highly significant correlation between the first and second rater (R^2=0.504, P<01), with the two observers differing by an average of 3.5% (±2.4 S.E.M.; Fig. 4C).

3.3. Assessment of morphological alterations resulting from gene knockout

To assess the applicability of this technique for anatomical phenotyping of genetically engineered mice, we used a FoxG1 gene-targeted knockout mouse line (FoxG1$^{+/-}$). FoxG1 encodes a transcription factor that regulates neurogenesis in the embryonic telencephalon as well as in the postnatal hippocampus [18,19]. In the central nervous system, neurogenesis is most pronounced from neural tube formation until birth and then, with the exception of the hippocampus and OB, decreases significantly throughout postnatal life. FoxG1$^{+/-}$ mice have been reported to be generally microencephallic, with the hippocampal and cortical regions [18,19] being most severely impacted. It was possible to obtain complete imaging datasets on eight prepared brain specimens in a total of 6 h. As expected, the hippocampus, OB, cortex and cerebellum of FoxG1$^{+/-}$ specimens were found to be significantly smaller compared with wild-type controls (Table 1). The effects of FoxG1 haploinsufficiency were particularly pronounced in the hippocampus and OB; regions of the brain continue to undergo neurogenesis throughout life, a process we have shown to be impaired in FoxG1$^{+/-}$ mice [19].

As a second and considerably more demanding test of this methodology, we investigated TrkB-haploinsufficient mice. TrkB is a member of the Trk tyrosine kinase receptor family and is found throughout the central nervous system [20]. TrkB is most highly expressed in the hippocampus and cerebral cortex [21], and is the primary receptor to which brain-derived neurotrophic factor binds [21,22]. The loss of

Table 1
Regional volumes (mm^3) for genetically engineered lines of mice

	Cortex, right hemisphere	Cerebellum	Hippocampus	Olfactory bulb
FoxG1 (wild type), *n*=4	59.4±(0.86)	46.9±(0.64)	16.6±(0.37)	8.2±(0.23)
FoxG1 (+/−), *n*=4	43.1±(0.99)*	43.5±(0.77)*	10.2±(0.29)*	6.2±(0.20)*
t-Statistic	*t* (5)=11.858	*t* (5)=3.200	*t* (6)=13.769	*t* (6)=6.341
TrkB (wild type), *n*=4	53.6±(0.42)	47.7±(1.88)	19.4±(0.63)	9.1±(0.47)
TrkB (+/−), *n*=4	56.9±(2.30)	50.3±(0.49)	17.8±(0.32)*	7.6±(0.40)*
t-Statistic	*t* (6)=1.410	*t* (6)=1.278	*t* (6)=2.238	*t* (6)=2.518

Data are presented as mean volumes in cubic millimeters±(S.E.M.). For statistical analysis, Student's *t* test for small samples was used, with asterisks (*) indicating a one-tailed *P* value of <.05 when comparing the results from knockout animals with wild-type controls.

TrkB has been shown to alter postnatal hippocampal neurogenesis, as well as to impact cell morphology in hippocampal and cortical regions [22,23]. Adult $TrkB^{+/-}$ mice have previously been reported to have a decrease in total hippocampal volume of approximately 7% [24,25]. When comparisons were made between genotypes via MRM, we found a significant decrease in hippocampal volume of $TrkB^{+/-}$ mice of 9.2% (±2 S.E.M.; Student's *t* test; *t* (6) =2.283, *P*<.03; *n*=4; Table 1) compared to wild-type controls. Interestingly, we also found region-specific differences in brain volume in $TrkB^{+/-}$ mice that had not previously been reported. $TrkB^{+/-}$ mice were found to have a significant decrease in OB volume compared to wild-type controls, suggesting anatomical defects within this region (Student's *t* test; *t* (6)=2.518, *P*<.05; *n*=4 mice per group; Table 1). To investigate this finding in more detail, all mice that underwent MRI were previously injected with BrdU, a thymidine analog that is incorporated into the DNA of dividing cells. The mice were allowed to survive for 28 days post BrdU injection prior to sacrifice for imaging, which is a sufficient amount of time for newly born cells that had incorporated BrdU to differentiate into a mature neuronal phenotype [26]. Comparing the density of BrdU-labeled cells in the OB, we discovered an approximately 30% decrease in the survival of newly born BrdU-labeled cells (Student's *t* test; *t* (6) =3.644, *P*<.05; *n*=4 mice per group; Fig. 5). This impairment in cell survival may at least in part explain the observed decrease in OB volume (Table 1). It should also be noted that, despite reports describing alterations in cell morphology in the cortex and cerebellum in TrkB-haploinsufficient mice, no differences were found between genotypes for the cortical or cerebellar volume (Table 1).

4. Conclusions

The methodology described in this report demonstrates that quantitative MRM, specifically the evaluation of murine neuroanatomy from genetically engineered mice, is possible in 30 min at 3.0 T. By utilizing lower field strengths and taking advantage of both inherent and contrast agent-induced differences in relaxation times of structures of interest, images could be obtained with high CNRs making structural boundaries easily identifiable. The

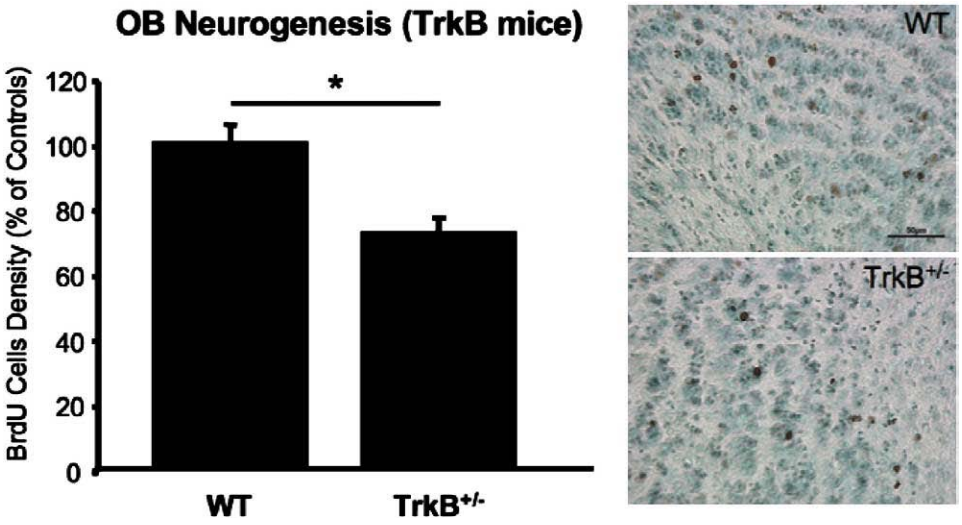

Fig. 5. Quantification of disruption in OB neurogenesis in TrkB-haploinsufficient mice. (Left) Bar graphs depicting the quantification of BrdU-positive cells in the granule cell layer of the OB for TrkB wild-type (+/+; *n*=4) and heterozygous (+/−; *n*=4) mice. (Right) Representative images of BrdU-labeled (brown) OB sections that were lightly counterstained with cresyl violet (see text for details).

selected image resolution of 100×78×78 μm was wholly adequate for highly reliable and accurate estimation of hippocampal volumes and approximates what is used for standard histological procedures of volume estimation (at typical sampling intervals of 120 μm). With these techniques, it was possible to accurately and rapidly identify volumetric differences by genotype and uncover novel underlying defects.

The ability to detect novel differences in phenotypic outcomes following a genetic manipulation was the primary goal of the present methods. By using information available a priori, such as gene expression patterns, it was possible in a targeted fashion to use MRM to quantify differences that were due to genetic disruption. In addition, quite often genetic manipulations have unanticipated effects on both region structure and function that may either be primary or secondary to the genetic manipulation, and therefore a whole brain scan may yield unexpected differences, as was the case in the OB of the TrkB heterozygous mice.

While in this study regional volume was measured through manual segmentation, the procedures described here may be advantageous for conducting similar studies in which automated segmentation is utilized. For most autosegmentation algorithms designed to date, co-registered images obtained with multiple scan sequences, resulting in different contrast, are required for accurate analysis. The ability to generate images with different contrast rapidly at lower fields could be highly advantageous for high-throughput work.

The methods described herein are either widely available or can easily be duplicated in most laboratories around the world. The generation of image contrast using materials other than, or in combination with, standard gadolinium-based agents appears to be an area ripe for further investigation. The overall methodology described in this report may help MRM further realize its full potential, which was first proposed more than 30 years ago [27].

Acknowledgments

We thank Professor Gary H. Glover of Stanford University for providing the specific version of the MP-RAGE pulse sequence used for this work.

References

[1] Benveniste H, Blackband S. MR microscopy and high resolution small animal MRI: applications in neuroscience research. Prog Neurobiol 2002;67:393–420.

[2] Johnson GA, Cofer GP, Gewalt SL, Hedlund LW. Morphological phenotyping with MR microscopy: the visible mouse. Radiology 2002; 222:789–93.

[3] Johnson GA, Thompson MB, Drayer BP, Bone SN. Magnetic resonance microscopy in neurologic models. Acta Radiol Suppl 1986;369:267–8.

[4] Johnson GA, Thompson MB, Gewalt SL, Hayes CE. Nuclear magnetic resonance imaging at microscopic resolution. J Magn Reson 1986;68: 129–37.

[5] Ballon DJ, Graham MC, Miodownik S, Koutcher JA. Doubly tuned solenoidal resonators for small animal imaging and spectroscopy at 1.5 tesla. Magn Reson Med 1989;7:155–62.

[6] Koretsky AP. New developments in magnetic resonance imaging of the brain. J Am Soc Exp Ther 2004;1:155–64.

[7] Van de Ven RCG, Hogers B, van den Maagdenberg AMJM, de Groot HJM, Ferrari MD, Frants RR, et al. T_1 relaxation in in vivo mouse brain at ultra-high field. Magn Reson Med 2007;58:390–5.

[8] de Graaf RA, Brown PB, McIntyre S, Nixon TW, Behar KW, Rothman DL. High magnetic field water and metabolite proton T1 and T2 relaxation in rat brain in vivo. Magn Reson Med 2006;56: 386–94.

[9] Bath KG, Voss HU, Dyke JP, Jing D, Anderson S, Lee F, et al. Rapid quantitative magnetic resonance microscopy of excised anatomy in the transgenic mouse at 3.0 tesla. Proceedings of the International Society of Magnetic Resonance in Medicine Fifteenth Annual Meeting, 15; 2007. p. 3653.

[10] Hanashima C, Shen L, Li SC, Lai E. Brain factor-1 controls the proliferation and differentiation of neocortical progenitor cells through independent mechanisms. J Neurosci 2002;22:6526–36.

[11] Klein R, Pajiada LF, Coulier F, Barbacid M. trkB, a novel tyrosine protein kinase receptor expressed during mouse neural development. EMBO J 1989;8:3701–9.

[12] Hoult DI, Deslauriers R. A high-sensitivity, high-B1 homogeneity probe for quantitation of metabolites. Magn Reson Med 1990;16:411–7.

[13] Voss HU, Ballon DJ. High-pass two-dimensional ladder network resonators for magnetic resonance imaging. IEEE Trans Biomed Eng 2006;53:2590–3.

[14] Mugler III JP, Brookeman JR. Three-dimensional magnetization-prepared rapid gradient-echo imaging (3D MP-RAGE). Magn Reson Med 1990;15:152–7.

[15] Paxinos G, Franklin KBJ. The Mouse Brain in Stereotaxic Coordinates. 2nd Edition. San Diego, CA: Academic Press; 2001.

[16] Gunderson HJ, Jensen EB. The efficiency of systematic sampling in stereology and its prediction. J Microsc 1987;147:229–63.

[17] Johnson GA, Ali-Sharief A, Badea A, Brandenburg J, Cofer G, Fubara B, et al. High-throughput morphologic phenotyping of the mouse brain with magnetic resonance histology. NeuroImage 2007;37:82–9.

[18] Xuan S, Baptista CA, Balas G, Tao W, Soares VC, Lai E. Winged helix transcription factor BF-1 is essential for the development of the cerebral hemispheres. Neuron 1995;14:1141–52.

[19] Shen L, Nam HS, Song P, Moore H, Anderson SA. FoxG1 haploinsufficiency results in impaired neurogenesis in the postnatal hippocampus and contextual memory deficits. Hippocampus 2006;16:875–90.

[20] Masana Y, Wanaka A, Kato H, Asai T, Tohyama M. Localization of trkB mRNA in postnatal brain development. J Neurosci Res 1993;35: 468–79.

[21] Chao MV. Neurotrophins and their receptors: a convergence point for many signalling pathways. Nat Rev Neurosci 2003;4:299–309.

[22] Lu B, Figurov A. Role of neurotrophins in synapse development and plasticity. Rev Neurosci 1997;8:1–12.

[23] Bath KG, Mandairon N, Rajagopal R, Kapoor R, Jing DQ, Chen ZY, et al. Variant brain-derived neurotrophic factor (Val66Met) alters adult olfactory bulb neurogenesis and spontaneous olfactory discrimination. J Neurosci 2008;28:2383–93.

[24] Linnarsson S, Willson CA, Ernfors P. Cell death in regenerating populations of neurons in BDNF mutant mice. Brain Res Mol Brain Res 2000;75:61–9.

[25] von Bohlen und Halbach O, Minichiello L, Unsicker K. Haploinsufficiency in trkB and/or trkC neurotrophin receptors causes structural alterations in the aged hippocampus and amygdala. Eur J Neurosci 2003;18:2319–25.

[26] Winner B, Cooper-Kuhn CM, Aigner R, Winkler J, Kuhn HG. Long-tern survival and cell death of newly generated neurons in the adult rat olfactory bulb. Eur J Neurosci 2002;16:1681–9.

[27] Lauterbur PC. Image formation by induced local interactions—examples employing nuclear magnetic resonance. Nature 1973;242:190–1.